# Plastid-localized amino acid metabolism coordinates rice ammonium tolerance and nitrogen use efficiency

**Wei Xuan** ( wexua@njau.edu.cn )

MOA Key Laboratory of Plant Nutrition and Fertilization in Lower-Middle Reaches of the Yangtze River and State Key Laboratory of Crop Genetics and Germplasm Enhancement, Nanjing Agricultural Univers

**Yuanming Xie**

MOA Key Laboratory of Plant Nutrition and Fertilization in Lower-Middle Reaches of the Yangtze River and State Key Laboratory of Crop Genetics and Germplasm Enhancement, Nanjing Agricultural Univers

**Yuanda Lv**

Dept. Ecology and Evolutionary Biology, University of California, Irvine https://orcid.org/0000-0002-6640-5989

**Letian Jia**

State Key Laboratory of Crop Genetics and Germplasm Enhancement and MOA Key Laboratory of Plant Nutrition and Fertilization in Lower-Middle Reaches of the Yangtze River, Nanjing Agricultural Univers

**Lulu Zheng**

State Key Laboratory of Crop Genetics and Germplasm Enhancement and MOA Key Laboratory of Plant Nutrition and Fertilization in Lower-Middle Reaches of the Yangtze River, Nanjing Agricultural Univers

**Yonghui Li**

State Key Laboratory of Crop Genetics and Germplasm Enhancement and MOA Key Laboratory of Plant Nutrition and Fertilization in Lower-Middle Reaches of the Yangtze River, Nanjing Agricultural Univers

**Ming Zhu**

State Key Laboratory of Crop Genetics and Germplasm Enhancement and MOA Key Laboratory of Plant Nutrition and Fertilization in Lower-Middle Reaches of the Yangtze River, Nanjing Agricultural Univers

**Mengjun Tian**

Department of Plant Pathology, Nanjing Agricultural University

**Ming Wang**

Department of Plant Pathology, Nanjing Agricultural University

**Weicong Qi**

Wageningen University

**Long Luo**

State Key Laboratory of Crop Genetics and Germplasm Enhancement and MOA Key Laboratory of Plant Nutrition and Fertilization in Lower-Middle Reaches of the Yangtze River, Nanjing Agricultural Univers

**Hugues De Gernier**

Department of Plant Biotechnology and Bioinformatics,VIB-UGent Center for Plant Systems Biology,Ghent University

**Pierre-Mathieu Pelissier**

Department of Plant Biotechnology and Bioinformatics,VIB-UGent Center for Plant Systems Biology,Ghent University

**Hans Motte**

Department of Plant Biotechnology and Bioinformatics,VIB-UGent Center for Plant Systems Biology,Ghent University

**Shaoyan Lin**

State Key Laboratory of Crop Genetics and Germplasm Enhancement and MOA Key Laboratory of Plant Nutrition and Fertilization in Lower-Middle Reaches of the Yangtze River, Nanjing Agricultural Univers

**Le Luo**

State Key Laboratory of Crop Genetics and Germplasm Enhancement and MOA Key Laboratory of Plant Nutrition and Fertilization in Lower-Middle Reaches of the Yangtze River, Nanjing Agricultural Univers

**Guohua Xu**

Nanjing Agricultural University https://orcid.org/0000-0002-3283-2392

**Tom Beeckman**

Department of Plant Biotechnology and Bioinformatics,VIB-UGent Center for Plant Systems Biology,Ghent University

---

**Article**

**Keywords:** Ammonium toxicity, Nitrogen use efficiency, Root elongation, ROHAN, Gln, Arg, Auxin, Oryza sativa L.

**Posted Date:** April 14th, 2022

**DOI:** https://doi.org/10.21203/rs.3.rs-1474062/v1



---

**Version of Record:** A version of this preprint was published at Nature Plants on August 21st, 2023. See the published version at https://doi.org/10.1038/s41477-023-01494-x.

# Abstract

Ammonium toxicity affecting plant metabolism and development is a worldwide problem impeding crop production. Remarkably, rice (Oryza sativa L) favors ammonium as its major nitrogen source in paddy fields. We set up a forward-genetic screen to decipher the molecular mechanisms conferring rice ammonium tolerance and identified the rohan mutant showing root hyper-sensitivity to ammonium due to a missense mutation in an arginine-succinate lyase-encoding gene. ROHAN localizes to plastids while its expression is induced by ammonium. ROHAN alleviates ammonium-inhibited root elongation by converting the excessive glutamine into arginine. Consequently, arginine leads to auxin accumulation in the root meristem thereby stimulating root elongation under high ammonium. Furthermore, we identified natural variation in the ROHAN allele between Japonica and Indica subspecies explaining their different root sensitivity towards ammonium. Finally, we show that ROHAN expression positively correlates with root ammonium tolerance and that nitrogen use efficiency and yield can be improved through a gain-of-function approach.


# Introduction

Nitrogen (N) is one of the essential nutrients for plant growth and crop yield because its metabolism *in vivo* leads to the production of diverse organic compounds, such as proteins, nucleic acids, chlorophyll, and plant hormones. Nitrate ($NO_3^-$) and ammonium ($NH_4^+$) are two primary inorganic N sources for plants. Nitrate is reduced into $NH_4^+$ by ferredoxin-dependent nitrite reductases, consuming NADH or NADPH as reductants, while $NH_4^+$ can be directly incorporated into amino acids via the GS-GOGAT pathway[1]. Thus $NH_4^+$ is considered a more efficient and economical N fertilizer than $NO_3^-$ to promote crop yield[2]. However, excessive $NH_4^+$ causes severe toxic effects on plant shoot and root growth[3]. Because the intensive use of $NH_4^+$-based fertilizers in the past decades has resulted in dangerous accumulation of $NH_4^+$ in agricultural soils[4], improving plant tolerance to $NH_4^+$ is key to the enhanced utilization of $NH_4^+$ and improve N use efficiency (NUE).

The mechanism underlying plant $NH_4^+$ tolerance have been extensively investigated in *Arabidopsis* through genetic approaches, and $NH_4^+$ toxicity is suggested to be a consequence of repressed metabolic processes[3], protein glycosylation[5], chloroplast development[6], hormone metabolism[6–8], glucosinolate metabolism and Fe homeostasis[9]. Recent studies have also revealed that $NH_4^+$ toxicity is coupled with $NH_4^+$ uptake and glutamine (Gln) accumulation by reducing root apoplast pH and provoking severe acidic stress to *Arabidopsis*[10,11]. In *Arabidopsis* mutants showing reduced $NH_4^+$ uptake (for instance, the ammonium transporters *AMTs* quadruple mutant) or Gln synthesis (e.g. *gln2-1*), the toxic effects of $NH_4^+$ on seedling growth are vastly relieved. The $NH_4^+$ toxicity can also be alleviated when the NRT1.1-mediated nitrate influx is reduced or the SLAH3-mediated nitrate efflux is enhanced, which both increase

external nitrate levels to buffer the rhizosphere pH[12,13]. Together, these results suggest that root acidification is the primary cause of $NH_4^+$ toxicity in *Arabidopsis*.

Rice is considered as a $NH_4^+$ tolerant species since $NH_4^+$ is the primary N source for rice in the paddy field, where the nitrification process is low[14]. AMT-mediated $NH_4^+$ uptake plays a predominant role in promoting rice shoot growth and yield[15] but negatively regulates root system architecture, in particular by reducing rice root elongation and gravitropism[16,17]. Several studies suggested that the inhibitory effect of $NH_4^+$ on rice root elongation is probably due to its impact on the biosynthesis of plant hormones such as auxin, ethylene, and brassinosteroids, which are critical for sustaining root development[11,18,19]. Our recent work also showed that root acidification resulting from $NH_4^+$ uptake triggered the asymmetric auxin distribution in the root cap, leading to the loss of root gravitropism under high $NH_4^+$[11]. However, root elongation inhibited by $NH_4^+$ could not be fully mitigated by buffering the rhizosphere pH or by supplying external nitrate supply, thus suggesting a different impact of $NH_4^+$ in root development between *Arabidopsis* and rice.

In order to decipher the molecular machinery allowing rice to circumvent $NH_4^+$ toxicity on root growth, we employed a forward genetic approach and identified *ROOT HYPERSENSITIVE TO AMMONIUM NITROGEN* (*ROHAN*) as a key regulator of $NH_4^+$ tolerance in rice. We further show that *ROHAN* encodes a plastid-localized argininosuccinate lyase which metabolizes excessive Gln into arginine (Arg), by doing so, alleviating $NH_4^+$-inhibition of root elongation. Additionally, we show that a substitution in the *ROHAN* coding sequence present of a particular rice cultivar can confer root tolerance to high $NH_4^+$. Finally, we demonstrate that ROHAN not only help to cope with $NH4^+$ toxicity but also promotes rice yield and NUE under low and high N supplies, which represents an important target for rice molecular breeding of $NH_4^+$ tolerance and NUE.

# Results

### Rice *rohan* mutants display root growth hypersensitivity to ammonium

To discover the genetic control of rice root responses to $NH_4^+$, an EMS-mutagenized population (10,000 mutant lines) was generated starting from a local elite *Japonica* cultivar Wuyungeng 7 (hereafter designated as the wild-type). We then screened for mutants showing altered root length when grown in hydroponic solutions supplied with 2.5 mM $NH_4^+$, a concentration that is known to cause inhibition of seminal root (SR) elongation[11]. Because $NH_4^+$ uptake results in proton release[11], MES was supplemented in order to exclude root phenotypes caused by lowering pH. We identified one mutant displaying severely inhibited SR elongation when compared with the wild-type under high $NH_4^+$ supply (73.9% shorter than the wild-type SR length). In absence of N however, the mutant SR length was slightly shorter than the wild-type (35.9% decrease) (Fig. 1a and b). We further observed that the highest sensitivity of SR

elongation to $NH_4^+$ in the mutant occurred at 2.5 mM $NH_4^+$, and that SR elongation was less sensitive to varying $NO_3^-$ concentrations (Extended Data Fig. 1a). A time-course experiment moreover showed that the inhibitory effect of $NH_4^+$ on SR elongation in the mutant was more pronounced after three days of treatment than one day (Extended Data Fig. 1b). Furthermore, the root phenotype of this mutant was consistently observed in the paddy field supplied with low N (75 kg/ha urea) and high N supply (350 kg/ha urea) (Fig. 1e and f). Because of the striking inhibition of root growth under ammonium supply, we named the mutant *root hypersensitive to ammonium nitrogen* (*rohan*).

Root elongation is determined by the meristem cell division activity and the subsequent cell elongation. Thus, we investigated the root meristem development in *rohan* under different N conditions. Compared to the N-free control condition, $NH_4^+$ treatment caused a significant reduction of both meristem length and cortical cell number in wild-type, and this inhibitory effect on meristem division was enhanced in *rohan* (Fig. 1c and d). In contrast, the cortical cell elongation was not affected in *rohan* neither for N-free or $NH_4^+$ supply (Extended Data Fig. 1c and d). We further determined the root meristem activity of the mutant *rohan* by employing an EdU-based S-phase (DNA synthesis phase) assay[20]. $NH_4^+$ treatment led to weaker EdU signal in the root tips of both the wild-type and *rohan* than under N-free condition. Nevertheless, root meristems of *rohan* showed less EdU signal than wild-type under high $NH_4^+$ supply (Fig. 1c and d). These results indicated that root phenotype of *rohan* resulted from reduced meristem activity under high $NH_4^+$ supply.

Next, we investigated whether the hypersensitive *rohan* root response to $NH_4^+$ toxicity was caused by $NH_4^+$ accumulation and the herewith associated *in vivo* acidic stress. Transcription analysis showed that the respective expression levels of *AMT1.1*, *AMT1.2*, *AMT1.3*, and *AMT2.1* in the roots were similar between wild-type and *rohan* (Extended Data Fig. 2a). Consistently, the *rohan* mutation had a minor effect on $NH_4^+$ uptake of roots and it also showed a lower root proton influx than the wild-type (Fig. 1g, and Extended Data Fig. 2b). Additionally, *rohan* exhibited an equal reduction in root elongation under low pH treatment as wild-type (Extended Data Fig. 2c and d). These results therefore suggested that the root response of *rohan* to $NH_4^+$ was most likely not a consequence of $NH_4^+$ uptake and acidic stress.

## *ROHAN* encodes an N-responsive and plasmid-localized argininosuccinate lyase

To identify the mutation causing the root hypersensitivity of *rohan* to ammonium, we performed a MutMap analysis using an $F_2$ segregating population of *rohan* backcrossed with the parental line. We found that the *rohan* mutation was inherited as a single recessive mutation by observing the root phenotype of $F_1$ progeny and self-pollinated $F_2$ population. The seedlings of the $F_1$ progeny showed a parent-like root sensitivity to $NH_4^+$ treatment, and $F_2$ progeny phenotypically segregated in nearly 3:1 ratio for a respective $NH_4^+$ sensitive and hypersensitive root phenotype ($\chi 2 = 0.58$; $P < 0.05$) (Extended Data

Fig. 3a and b). Detailed bulked genomic sequencing and MutMap analysis on the $F_2$ progeny identified a non-synonymous single base change (C to T) at position 1706-bp downstream of the start codon of *Os03g05500* (Fig. 2a and Extended Data Fig. 3c). The gene encodes an argininosuccinate lyase (ASL), which is known to catalyzes the conversion of argininosuccinate into arginine and fumarate[21]. *ROHAN/ASL* gene is highly conserved within the plant kingdom (Extended Data Fig. 4a).

In rice, ROHAN/ASL contains seven exons, and the mutation in *rohan* results in a Pro211Leu (P211L) substitution located at the third exon (Fig. 2a). Pro211 is highly conserved among plant species (Extended Data Fig. 4c). By structural modelling the ROHAN/ASL protein based on the ASL crystal structure in *Bacillus coli*, we found the Pro211 at the hinge region linking protein domains (Fig. 2f and Extended Data Fig. 4c). To confirm that the P211L mutation is responsible for ROHAN function and root response to $NH_4^+$, we further performed genetic complementation by transforming *rohan* mutants with VENUS-fused ROHAN/ASL wild-type protein driven by its native promoter (*proROHAN:ROHAN-VENUS rohan*). Over 24 individual lines were obtained, and lines with *ROHAN-VENUS* expression in the root showed identical root sensitivity to $NH_4^+$ as the wild-type (Fig. 2b and c). Additionally, knock-out lines of *ROHAN/ASL1*, generated by CRISPR-cas9, mimicked the root phenotype of *rohan* under high $NH_4^+$ supply (Fig. 2b and c). Thus, ASL is responsible for *rohan* root phenotype while its function is dependent on the Pro211 residue.

By generating a transcriptional reporter line of *ROHAN* in the wild-type background, we observed a strong expression of *proROHAN:GUS* in the root meristem and the stele of the elongation zone. *proROHAN:GUS* was also found to be expressed in lateral root primordia and emerged lateral roots (Extended Data Fig. 4b), indicating a critical role of ROHAN in regulating rice root development. In the complemented lines, the ROHAN-VENUS signal was also highly detected at the root meristem and localized to plastids at the cellular level (Fig. 2d). The Pro211Leu (P211L) did not affect the subcellular localization of ROHAN (Fig. 2e) and suggested the Pro211 residue is key to its protein function in plastids.

We next investigated whether *ROHAN* expression was regulated by external $NH_4^+$ supply. qRT-PCR analysis showed that *ROHAN* expression in roots gradually increased by $NH_4^+$ application over 24h, while it was less induced by $NO_3^-$ treatment (Fig. 2g). This was further confirmed by the expression analysis of *proROHAN:GUS,* showing a strong induction of *ROHAN* expression in the root meristem by $NH_4^+$ after 24h (Fig. 2h). All together, these data demonstrate that *ROHAN* is a $NH_4^+$ responsive gene that encodes a plasmid-localized protein regulating root development.

## Metabolic defect of $NH_4^+$/Gln conversion to Arg in *rohan* causes its root hypersensitivity to ammonium

The *ROHAN* encoded ASL has previously been shown to play a role in amino acid (AA) metabolism by catalyzing the last step of Arg biosynthesis. Furthermore, Arg produced by ASL is believed to be required

for normal root elongation in rice[22] suggesting a possible link between ROHAN function in plastids and root tolerance to $NH_4^+$. To address the latter, we measured the content of 20 free AAs in roots of *rohan* and wild-type under N-free condition and high $NH_4^+$ supply. $NH_4^+$ treatment increased the overall content of AAs, especially Asn and Gln both in wild-type and *rohan* roots (Extended Data Fig. 5a). Remarkably, upon high $NH_4^+$ supply, more Gln and free $NH_4^+$ accumulated in roots of the *rohan* and *rohan*$^{CR}$*4* mutants than in the wild-type. The opposite trend was observed for the Arg content, being more reduced in the mutants than in the wild-type roots (Fig. 3a). $NH_4^+$ is assimilated to Gln by Glutamine synthetase (GS), and Gln is subsequently converted to Arg by the Urea cycle (Fig. 3b)[23,24]. Thus, the increased Gln and $NH_4^+$ in *rohan* roots might be due to the perturbation of Arg synthesis. In the complementing line of *rohan*, the contents of Gln, $NH_4^+$ and Arg in the root were all recovered to the wild-type levels (Fig. 3a and Extended Data Fig. 5a), confirming that ROHAN acts on the conversion of $NH_4^+$/Gln to Arg.

Next, we questioned if the observed metabolic defect was associated with *rohan* root sensitivity to $NH_4^+$ by testing the effects of Gln and Arg application on root growth. We observed a substantial inhibition of SR meristem cell division and elongation at 0.3 mM Gln treatment in the wild-type. In *rohan* however, Gln concentration as low as 0.03 mM Gln already caused significant inhibition of SR meristem cell division and elongation (Fig. 3c, d, h, i and Extended Data Fig. 5g). This suggested that root elongation of *rohan* is hypersensitive to Gln, mimicking its response to $NH_4^+$. Interestingly, the addition of methionine sulfoximine (MSO), a potent inhibitor of GS[25], restored SR elongation in both the wild-type and *rohan* under high $NH_4^+$ supply (Fig. 3c and d). We further used CRISPR-Cas9 to generate quadruple mutants of *AMTs* (*qko*)[26] and a *gs1;1* single mutant, which are defective in Gln synthesis (Extended Data Fig. 5b and c)[27]. Both *qko* and *gs1;1* mutants showed resistance to $NH_4^+$ treatment towards SR elongation (Fig. 3e and f) indicating that Gln accumulation is a major factor responsible for $NH_4^+$ toxicity to root elongation in rice.

Intriguingly, the arrested SR meristem cell division and elongation in *rohan* under high $NH_4^+$ could be rescued by the supply of Arg, with the optimum concentration at 0.3 mM, while it had a minor effect on SR meristem cell division and elongation in the wild-type (Fig. 3d, h, i, and Extended Data Fig. 5d). However, external Arg supplies could not rescue the $NH_4^+$- and Gln-inhibited SR elongation in the wild-type (Extended Data Fig. 5e and f), suggesting that endogenous Arg, produced by ROHAN, is required for root elongation under high $NH_4^+$. Thus, we concluded that the biological function of ROHAN in converting excessive $NH_4^+$/Gln to Arg *in vivo*, enables the alleviation of $NH_4^+$ inhibited rice root elongation.

## ROHAN promotes nitrogen metabolism and photosynthesis under high ammonium supply

We next aimed to unveil the mechanism underlying ROHAN-mediated root tolerance to $NH_4^+$ by performing RNA-seq analysis of root meristems in *rohan* and wild-type under N-free condition and $NH_4^+$ supply. In agreement with the hypersensitive root phenotypes of *rohan* mutants under high $NH_4^+$, a more diverged transcriptional pattern between *rohan* mutants and the wild-type under high $NH_4^+$ compared to N-free was observed (Extended Data Fig. 6a).

To specify the molecular pathways downstream of ROHAN, we analyzed differentially expressed genes in the wild-type and *rohan* under $NH_4^+$ and N-free conditions. $NH_4^+$ treatment led to a higher number of differentially expressed genes in *rohan* than wild-type after 1d treatment, and the number of differentially expressed genes in *rohan* was increased mainly after 3 days of treatment (Extended Data Fig. 6b). Gene set enrichment analysis of these differentially expressed genes based on GO and KEGG suggested that the N metabolism pathway was significantly affected in *rohan* (Extended Data Fig. 6c), consistent with its altered amino acid metabolism. Interestingly, genes associated with ammonium assimilation and Gln synthesis, including three GS1 members and GDH1, were all found to be significantly down-regulated in *rohan* under $NH_4^+$ treatment (Extended Data Fig. 6d and e), which might result from a feedback inhibition by the accumulated Gln in *rohan*.

In addition, photosynthesis pathway genes were also significantly enriched in *rohan* under high $NH_4^+$ (Extended Data Fig. 6b). Increasing N supply can promote photosynthesis in rice[28,29]. Consistently, high $NH_4^+$ supply significantly induced photosynthetic rate, transpiration rate, stomatal conductance and PSII in wild-type seedlings, severely repressed in *rohan*, correlating with retarded shoot growth in *rohan* mutants under $NH_4^+$ supply (Extended Data Fig.7b). The photosynthesis and shoot growth deficiency in *rohan* was recovered in the complementation line or by external Arg supply (Extended Data Fig.7a). These results show the importance of ROHAN for efficient AA metabolism in photosynthesis.

## The *rohan* root response to $NH_4^+$ is mediated by auxin metabolism

Interestingly, gene set enrichment analysis of differentially expressed genes revealed that hormone metabolism was also affected in *rohan* under high $NH_4^+$ (Extended Data Fig. 8a). Among plant hormones, auxin plays a crucial role in regulating root elongation and responses to N sources and photosynthesis[30,31]. The expression of several genes involved in auxin conjugation (i.e., GH3s) and auxin signaling (i.e., *ARF2*, *IAA6*, *IAA14*, and small auxin-up RNAs, SAURs) was found to be down-regulated in *rohan* under high $NH_4^+$ (Fig. 4a). *GH3s* and *SAURs* are auxin-inducible genes[32], thus the changes in their expression indicated altered endogenous auxin levels in *rohan*. By measuring endogenous IAA content, we indeed detected a significant reduction of IAA content in the root tip of *rohan* as compared to that of in the wild-type under high $NH_4^+$supply, while it was only slightly reduced in *rohan* under N deficiency (Extended Data Fig. 8b). In the complementation line of *rohan*, IAA content in the root tip was fully

recovered (Extended Data Fig. 8b), showing the importance of ROHAN for endogenous auxin metabolism in the root tip.

To reveal spatial changes in auxin levels in root tips, we introduced *DR5rev:3xVENUS*, a sensitive auxin reporter[33], into *rohan* mutants by crossing. The DR5 signal was strong in the root epidermis and stele of both the wild-type and *rohan* in N-free condition. Under high $NH_4^+$ treatment, wild-type roots had a lower DR5 signal in the stele but an increased signal in the epidermis, whereas it almost disappeared from the root stele and epidermis of *rohan*. Interestingly, exogenous Arg elevated DR5 expression in the root stele and epidermis of *rohan* mutants (Fig. 4b, c and Extended Data Fig. 8c), corresponding to its effect in restoring SR elongation in *rohan* mutants. These results indicate that the changes of auxin levels in the root tip are correlated with the ROHAN-mediated SR elongation in response to $NH_4^+$.

Regulation of the root meristem activity and root elongation in response to N sources is mediated by auxin efflux carrier PIN-dependent polar auxin transport (PAT)[34]. Accordingly, we also found that several PIN encoding genes were transcriptionally repressed in *rohan* mutants under high $NH_4^+$ (Fig. 4a). We further validated the role of PINs in mediating *rohan* root response to $NH_4^+$ by using two well-characterized potent polar auxin transport inhibitors, 1-N-naphthylphthalamic acid (NPA) and BUM[35,36], in order to bypass the functional redundancy of PIN proteins. Under high $NH_4^+$ supply, *rohan* mutants showed higher sensitivity to NPA and BUM with respect to SR elongation, as this was completely arrested at low concentration of NPA and BUM (Fig. 4d and e). Following inhibition of SR elongation by NPA, NPA treatment resulted in a higher accumulation of DR5 expression in the root epidermis of the wild-type upon $NH_4^+$ treatment (N-free), while this induction was blocked in *rohan*. Moreover, exogenous IAA failed to trigger DR5 expression and root elongation in *rohan* mutants, suggesting a complete suppression of PIN activity in *rohan* mutants (Fig. 4b and Extended Data Fig. 8c). We further generated a CRISPR-Cas9 knock-out mutant of *PIN1a* and *PIN1b*, whose expression abundances were significantly repressed in *rohan* mutants under high $NH_4^+$. The *pin1apin1b* mutants showed shorter root meristems and SRs, mimicking the *rohan* mutant root phenotype (Fig. 4g and i), confirming the requirement of PIN-mediated polar auxin transport for the ROHAN-dependent effect on SR elongation. Altogether, our data demonstrated a critical role of auxin metabolism and polar auxin transport underlying ROHAN-controlled root tolerance to ammonium stress.

## *ROHAN* allele confers rice root tolerance to $NH_4^+$ toxicity

Because of the significant role of ROHAN in $NH_4^+$ root tolerance, we further investigated its genetic variation in rice germplasm. By nucleotide diversity ($\pi$) and *Fst* analysis, we found evidence for decreased nucleotide diversity of *ROHAN* in the *japonica* and *indica* subpopulations as compared to the wild rice population (*Oryza rufipogon*), while regions around the ROHAN locus showed significant differentiation between subspecies *japonica* and *indica*, indicative for a possible result of selective pressure during

domestication (Fig. 5a and b). Detailed analysis showed 37 SNP variants, including 35 introns, one missense, and one synonymous within the *ROHAN* gene. We further focused on the missense SNP (Chr3:10847318, c.3972A>G), which showed apparent *Indica* (94.91%)-*Japonica* (96.76%) differentiation and led to a Lys470Arg substitution (Fig. 5d and e). The allele frequency of the SNP from *japonica*, *indica I*, *indica II*, *indica III*, *aus*, and *aromas* subpopulations were calculated and shown on the geographic map (Fig. 5c).

To validate the function of the SNP, we randomly selected in total 100 $SNP^{A}$-variant and $SNP^{G}$-variant accessions to evaluate their root sensitivity to high $NH_4^+$. Our results revealed a higher root sensitivity to $NH_4^+$ in $SNP^{G}$-variant accessions than $SNP^{A}$-variant accessions (Fig. 5f). Furthermore, *ROHAN* expression in $SNP^{G}$-variant accessions was less induced than $SNP^{A}$-variant accessions by high $NH_4^+$ (Fig. 5g). These results suggest that the SNP variation of *ROHAN* might be associated with transcriptional responses and SR elongation to $NH_4^+$. To experimentally validate this possibility, we further conducted allelic complementation by transforming $SNP^{G}$-variant (*proROHAN:ROHAN*$^{K470R}$, with only one missense SNP difference from the *Japonica* cultivar Wuyungeng 7 genome) into the *rohan*. Unlike the $SNP^{A}$-variant, which could restore SR elongation (Fig. 2b and c), while independent $SNP^{G}$-variant lines failed to rescue the SR elongation under high $NH_4^+$ supply (Fig. 5h and i), demonstrating that the natural *ROHAN* variants cause the divergence of the root tolerance to $NH_4^+$.

### *ROHAN* expression determines the rice tolerance to $NH_4^+$ toxicity and nitrogen use efficiency

Since *ROHAN* expression is correlated with root tolerance to $NH_4^+$, we further generated overexpression lines of *ROHAN (UBIL:ROHAN*) in a *rohan* background. Two independent *UBIL:ROHAN* lines, which had higher *ROHAN* expression (Extended Data Fig. 9b), showed longer SR than the wild-type upon different increasing $NH_4^+$ concentrations (2.5mM ~ 10mM) (Fig. 6a and b). In contrast, *rohan* displayed lower expression of *ROHAN* in roots and shorter SRs than wild-type (Extended Data Fig. 9b). These results underline once again the importance of *ROHAN* expression for root tolerance to $NH_4^+$.

We further planted the mutant and overexpression lines of *ROHAN* in the paddy field supplied with low (75 kg/ha), moderate (150 kg/ha), and high nitrogen (350 kg/ha). Compared to the wild-type, *ROHAN* overexpression led to a significant increase in tiller number, grain yield, grain proteins and nitrogen use efficiency under all N conditions, whereas *rohan* mutants showed lower tiller number, yield, grain proteins and NUE (Fig. 6c and d). Collectively, these results show that *ROHAN* expression positively correlates with root tolerance to high $NH_4^+$ and NUE.

# Discussion

Ammonium nitrogen can cause severe toxic effects on various plant physiological and developmental processes. In particular, $NH_4^+$ represses growth of the root system, which in turn leads to reduced nutrient and water uptake and therefore dramatically decreases crop yield. Improving plant tolerance to $NH_4^+$ thus represents a promising strategy to improve crop nitrogen use efficiency and yield. Although previous studies in rice have shown that reduced ammonium uptake or Gln synthesis could considerably alleviate the $NH_4^+$-inhibition of root growth, they also reported on retarded shoot growth, indicating an antagonistic interplay between $NH_4^+$ tolerance and NUE[26,37]. Here, we identified *ROHAN*, a gene encoding a plastid-localized ASL, essential in determining the $NH_4^+$ tolerance of rice roots. Our study revealed that $NH_4^+$ toxicity impeding rice root growth results from the accumulation of $NH_4^+$/Gln in roots. *ROHAN/ASL* is transcriptionally induced in the root meristem by $NH_4^+$ and facilitates the conversion of over-accumulated $NH_4^+$/Gln into Arg, which is essential for auxin homeostasis and root elongation under high $NH_4^+$ (Fig. 6e). Significantly, induction of *ROHAN* expression not only promotes rice root tolerance to $NH_4^+$ but also increases the NUE and yield under low and high N supplies in the paddy field. Therefore, our results suggest that the ROHAN-mediated Gln to Arg conversion coordinates root tolerance to $NH_4^+$ toxicity and NUE.

Amino acids are a primary storage form of N and exert diverse functions in plant development and defense[38]. $NH_4^+$ is assimilated via the GS-GOOAT pathway into Gln and further converted into other amino acids. The *ROHAN* encoded ASL is one of the rate-limiting enzymes of the urea cycle and is utilized in the production of arginine[21]. ROHAN shares the same plastidial localization with GS1;1[10] (Fig. 2), a critical enzyme for Gln synthesis. By analyzing the amino acid content, *ROHAN* was found to act specifically in the conversion pathway of Gln to Arg (Fig. 3), indicating a critical role of the urea cycle in Gln metabolism in plastids. In *Arabidopsis*, the elevated Gln content and root apoplast acidification by high $NH_4^+$ supply has been suggested as the primary cause of $NH_4^+$ toxicity[10]. Consistently, Gln had a similar inhibitory effect on root growth in rice, and *rohan* mutant roots show hypersensitive to external Gln supply, which can be suppressed when Gln synthesis is attenuated (Fig. 3). These results demonstrate that $NH_4^+$-induced accumulation of endogenous Gln is a common mechanism underlying $NH_4^+$ toxicity in rice root development. However, *rohan* mutant roots exhibited normal sensitivity to low pH (Extended Data Fig. 2), arguing that ROHAN-mediated root tolerance to $NH_4^+$ is unlikely linked to root acidification.

The regulation of N in plant root development is mediated by phytohormones such as auxin, ethylene, and brassinosteroid[11,39,40]. Auxin is a prominent regulator of root meristem activity and root elongation, and also interacts with other hormones to regulate root development[41]. Our transcriptome data revealed a robust transcriptional regulation of ROHAN in auxin signaling pathways (Fig. 4). We demonstrated that *ROHAN* plays a role in maintaining high auxin levels and spatial distribution at the root tip, required for root elongation under high $NH_4^+$. Local auxin accumulation is mediated by auxin efflux carrier PIN-dependent polar auxin transport. We further identified PIN1 as a downstream signaling component of

ROHAN. PIN1 activity is required for rice root meristem activity and SR elongation. *PIN1* is transcriptionally activated by ROHAN to facilitate the tissue-specific auxin accumulation at the root tip to stimulate root elongation. In *Arabidopsis*, high ammonium was also found to affect PIN activity.to adjust root growth[34]. Therefore, our study suggests a molecular link between the N metabolic pathway and the phytohormone signal in regulating rice root tolerance to ammonium. Further investigations will be needed to uncover the mechanism underlying the transcriptional regulation of ROHAN and $NH_4^+$ in auxin homeostasis.

*ROHAN* is highly conserved in various plant species. In this study, we further identified a natural variant of *ROHAN* ($SNP^A$) in rice that increases root tolerance to high external $NH_4^+$. This tolerance allele $SNP^A$ is mainly distributed in *Japonica* cultivars but is absent from *Indica* cultivars, correlating with the higher root tolerance of *Japonica* cultivars as compared to *Indica* cultivars (Fig. 5). As *ROHAN* expression is highly elevated by high $NH_4^+$ in *Japonica* cultivars in contrast to *Indica* cultivars, the elite allele of *ROHAN* might determine root tolerance to $NH_4^+$ toxicity through regulating its expression in response to external $NH_4^+$ supply.

In summary, we identified *ROHAN* as a critical regulator of $NH_4^+$ tolerance and NUE in rice. Our study reveals a molecular link between amino acid metabolism and root response to external N supply and suggests that polar auxin transport-mediated local auxin accumulation in the root meristem is required for ROHAN function. As rice varieties harboring the elite variant of *ROHAN* display a higher root tolerance to $NH_4^+$ without penalty in plant growth and yield, *ROHAN* may represent a potential candidate target for genetic editing or marker-assisted breeding to develop crop varieties tolerant to ammonium toxicity and help to increase rice NUE and yield under the large quantities of urea-based fertilizer. The identification of ROHAN therefore represents an important element to set up strategies to cope with the excessive use of N fertilizer that has resulted in several environmental issues, such as surface water eutrophication, groundwater pollution, greenhouse gas emission and soil acidification.

# Declarations


### Acknowledgements

We thank Hongye Qu, Xiaoli Dai and Kaiyun Qian for their technical help with the $^{15}N$ uptake assays and confocal imaging. This work was supported by China National Key Program for Research and Development (2021YFF1000403), National Natural Science Foundation (No. 32072658 and 31822047), Key Research and Development Program of Jiangsu Province (BE2020339), the Fundamental Research Funds for the Central Universities (KJYQ201903 and KYT201802), and Innovative Research Team Development Plan of the Ministry of Education of China (No. IRT_17R56) and the Research Foundation – Flanders (FWO): Bilateral Scientific Cooperation fund with China (NSFC) (No. G002817N).Y.M.X is supported by grant from the Chinese Scholarship Council (CSC, 201806850032).

### Author contributions

W.X. and T.B. directed the experiments. Y.M.X and Y.D.L. performed most of the experiments and analysis. L.T.J., L.L.Z, M.Z and L.L. helped with vector construction. Y.H.L helped with root section. M.J.T and M.W. helped the IAA content analysis. W.C.Q. helped the phenotyping analysis. H.D.G., and PM.P. helped the imaging. S.Y.L. helped the amino acid content analysis. All authors discussed the results and contributed to the finalization of the manuscript.

### Conflict of interest statement

All authors state no conflict of interest concerning this manuscript.

### Accession Numbers

Sequence data from this article can be found in the GenBank/EMBL databases under the following accession numbers: *ROHAN* (Os03g0305500), *AMT1;1* (Os04g0509600), *AMT1;2* (Os02g0620500), *AMT1;3* (Os02g0620600), *AMT2;1* (Os05g0468700), *GS1;1* (Os02g0735200), *PIN1a* (Os06g0232300), *PIN1b* (Os02g0743400).

## Online Methods

Plant materials

Rice (*Orzya sativa cv.* Wuyungeng7) seeds were mutagenized by treating them with 1.0% ethyl methylsulfonate (EMS) for 12 h as previously described[42]. $M_2$ seeds obtained from self-pollinated $M_1$ plants were used for the screening of $NH_4^+$-sensitive mutants based on root elongation at 2.5 mM ammonium. In brief, seeds from 10,000 $M_2$ lines were bulked, and 100 seeds were sown on a mesh in a 500ml volume cup. Young seedlings were subjected to ammonium treatment 3 days after germination with a hydroponic culture containing 2.5 mM ammonium. The root elongation of $M_3$ progeny was finally assessed in the same manner to confirm the $NH_4^+$-sensitive phenotype of the candidate mutant *rohan*. The rice *DR5rev:3xVENUS-N7* transgenic reporter line was previously described [33].

Plant growth conditions

Wild-type, mutants and transgenic rice seeds were surface-sterilized with 70% (v/v) ethanol for 2 min, followed by 30% (v/v) bleach containing 0.01% Tween 80 for 30 min. After 5 times washing with sterilized water, rice seeds were germinated at 37 ℃ for 3 days. Germinated rice seedlings were first grown in water for another 3 days in a growth chamber under a photoperiod of 14 h light (~ 200 μmol•$m^{-2}$•$sec^{-1}$ light density and ~ 60% humidity) and 10 h dark at 28 ℃. Subsequently, the rice seedlings with around 2 cm seminal roots were transferred to a hydroponic medium with modified Kimura B solution (500 ml volume for each cup with 10 seedlings, pH 5.5, 0.25g MES) for different treatments according to the previous study[11]. For N-free treatment, nitrogen sources $(NH_4)_2SO_4$ and $KNO_3$ were replaced with $K_2SO_4$ at a concentration of 1.25 mM. For $NO_3^-$ treatment, $(NH_4)_2SO_4$ was replaced with 2.5 mM $KNO_3$. The rice seedlings were treated for 6 days unless otherwise noted, and the hydroponic culture was refreshed every 2 days.

## Root phenotype analysis

The rice seedling roots were imaged with a 400dpi resolution by an EPSON Expression 11000XL scanner. Seedling roots were scanned before and after treatments. We then measured the seminal roots (SR) length using Fiji image analysis software (http://fiji.sc/). The SR elongation was finally calculated as the difference between the SR lengths after and before treatments.

## Genetic mapping of the *rohan* mutation

To identify the causal mutation, a $F_2$ population was generated by backcrossing *rohan* mutant with the parent Wuyungeng 7 then used for genetic mapping through a modified MutMap analysis[43]. We then performed whole genome re-sequencing of two $F_2$ segregant bulks: 20 individuals showing the parent phenotype and 20 others displaying the *rohan* $NH_4^+$-sensitive phenotype. Next, DNA was isolated from leaves for each individual using the DNeasy Plant Mini Kit (Qiagen) as previously described[42], and ultimately each DNA bulk was created by mixing equally individual DNA in order to reduce sequencing bias. Sequencing libraries with an average insert size of approximately 350–500 bp were constructed using the Illumina DNA Prep Kit and sequenced with PE150 mode using Illumina NovaSeq 6000 platform (Zhejiang Annoroad Biotechnology Co., Ltd., China). Raw FASTQ data were trimmed using Fastp v0.20[44], with sequencing adapters, low-quality bases, and short reads (<40 bp). Cleaned data were then aligned to the rice reference genome (IRGSP1.0, https://rapdb.dna.affrc.go.jp/) using BWA v0.7.17[45]. PCR duplication was removed by Sambamba v0.8.1[46]. SNP calling was performed using GATK v4.2.1[47], and all variants were scored by ED (Euclidean distance) and fitted by sliding window approach[43]. $ED^4$ was then calculated by raising ED to the fourth power to decrease noise. Candidate causal mutations with significance at the 95% confidence interval were finally identified. Data availability of the raw Whole-

genome sequencing (WGS) datasets, including parents and bulked DNA pools, have been deposited on NCBI BioProject (https://www.ncbi.nlm.nih.gov/bioproject) under the accession number PRJNA808438

## RNA-seq analysis

Roots from the wild-type and *rohan* mutant seedlings, treated with or without high $NH_4^+$ for 1 d and 3 d, were collected with three independent biological repeats for RNA-seq analysis. Total RNA was extracted using TRIzol reagent and digested with RNase-free DNase (Qiagen, Germany) according to the manufacturer's instructions. RNA was then purified and concentrated using an RNeasy column (Takara, Japan). RNA integrity numbers (RINs) were assessed by an Agilent 2100 bioanalyzer (Agilent Technologies, United States). The quantification of RNA was done using a Qubit 4 Fluorometer (Thermo Fisher Scientific Company, Germany). Purification of the poly-A mRNA and construction of the cDNA realized with the TruSeq RNA Library Preparation Kit (Illumina, United States). RNA sequencing was finally performed using the Illumina NovaSeq 6000 platform with PE150 (Zhejiang Annoroad Biotechnology Co., China).

RNA-seq datasets were then analyzed following a custom protocol previously published[48]. Raw data were also cleaned using Fastp v0.20[44]. Cleaned reads were aligned to the rice reference genome using STAR v2.7.8a with a splicing-aware method and two-pass mode[49]. The aligned reads were separately assembled into transcripts for each sample with the reference annotation-based transcript (RABT) assembly algorithm and generated an updated transcript annotation with GTF-formatted file using StringTie v2.1.3[50]. Finally, the expression level of genes was quantified and normalized with the above-updated GTF file using HTSeq, respectively[51]. Only the genes with an FPKM (fragments per kilobase of transcript per million fragments mapped) >1 in at least six samples were used for downstream gene expression analysis. DESeq2 was used to perform pairwise comparisons between conditional samples to identify differentially expressed (DEG) genes with the updated GTF file[52]. In our study, genes were considered as differentially expressed according to the following criteria: Log2 (Fold change) $\geq 1$ and the adjusted *p*-value < 0.05. Raw RNA-Seq datasets were also available on NCBI BioProject under PRJNA808101.

Venn diagrams and heatmaps were plotted from the differentially expressed genes using custom R scripts. Enrichment analysis based on GO and KEGG databases was carried out using PlantGSAD[53]. The Benjamini–Yekutieli method was used for *P*-value adjustment. Besides, clusterProfiler v3.14, a gene set enrichment analysis (GSEA) method[54], was further employed to determine if a prior defined set of genes such as nitrogen metabolism and plant hormone signal transduction shows concordant differences in response to $NH_4^+$ treatment between the mutant and the wild-type.

## Allelic variation and local adaption analysis

For allelic variation analysis of *ROHAN*, SNP datasets of 446 accessions of common wild rice (*Oryza rufipogon*) and 3K Rice Genomes Project were obtained from a previous study[55,56]. The nucleotide diversity (*Pi*) and *Fst* statistics were calculated and fitted with the sibling window method (window size:2 kb; step size:1 kb) for wild rice and rice subpopulations using VCFtools v.0.1.17[57]. Functional effects of variants from *ROHAN* and its surrounding regions (with 2 Kb flanking sequence on both sides) were predicted by SNPeff v4.3[58]. Allele frequency of missense SNP (Chr3:10847318) from six rice subgroups (japonica, indica I, indica II, indica III, aromatic and aus) of the 3,000 varieties were calculated and integrated into a geographical map according to their subpopulation and origin information from the Rice SNP-Seek Database (https://snp-seek.irri.org). Moreover, SR length and expression abundance corresponding to different alleles were also measured from a selection of 50 Japonica and 50 Indica varieties.

## Plastid construction and plant transformation

The Gateway system® (Invitrogen, Carlsbad, CA, USA) was employed to generate most genetic constructs. For transcriptional fusions, first, ~2k promoter fragments upstream of the start codon were amplified by PCR from genomic DNA and cloned into *pdonrp41R* by Bp reactions. Second, the *ROHAN* open reading frame with or without stop codon was amplified from genomic DNA and was cloned into *pDONR221* or *pDONR2F3R*, respectively. Subsequently, the vectors were introduced into different expression vectors by LR reactions. The expression vectors *pmk7snfm14GW*, *pHb7m34GW* and *pHb7m24GW* were respectively used for the promoter-GUS fusion, the complementation of the mutant and generating the overexpression lines.

To generate *pCRISPR-OsROHAN*, *pCRISPR-OsGS1;1* and *pCRISPR-OsPIN1a, pCRISPR-OsPIN1b* gene-editing constructs, the corresponding target sequences were blasted by CRISPR-GE (http://skl.scau.edu.cn/home/), and cloned into guide RNA (sgRNA) expression cassettes by overlapping PCR, the fragments were subsequentially cloned into the BsaI site of the pYLCRISPR/Cas9-MH vector.

All constructs were verified by DNA sequencing analysis. The primers used are listed in the Supplementary Table S1. *pUBIL:ROHAN*, *pROHAN:ROHAN1:VENUS* and *pROHAN:VENUS;ROHAN* were transformed into the *rohan* mutant. *pYLCRISPR/Cas9-MH-ROHAN*, *proROHAN:GUS* and *pCRISPR-OsPIN1a, pCRISPR-OsPIN1b* were transformed into the wild-type. *pYLCRISPR/Cas9-MH-OsGS1;1* was transformed into Nipponbare. All plasmids were transformed into rice plants using Agrobacterium-mediated transformation[59].

## Histochemical analysis and microscopy

GUS assays were done as previously described[60]. Roots were imaged with a Leica DM2500 microscope (Leica Microsystems, Wetzlar, Germany). For the anatomical sections, GUS-stained samples were fixed overnight and embedded following a published protocol[61].

*DR5rev:VENUS-N7* expression in the root tip of rice was observed with a Leica SP8 laser-scanning microscope equipped with a white laser and hybrid laser detectors. The root tips of rice *DR5rev:3xVENUS-N7* transgenic rice seedlings grown under different treatments were cleaned with a modified ClearSee method preceding confocal imaging as previously described[11]. Rice root meristems were imaged using a modified mPS-PI staining to clear and visualize the cell organization of rice SR tips[11].

## RNA extraction and quantitative real-time PCR analysis

Total RNA was isolated using the plant RNA purification reagent (Invitrogen). cDNA was synthesized from 1 µg of RNA with the Advantage® RT-for-PCR Kit (TaKaRa) according to the manufacturer's instructions and was diluted 20 times for subsequent quantitative (q)PCR. Real-time PCR was done in Real-time PCR machine (LightCycler 480, Roche Diagnostics) according to the manufacturer's manuals in a reaction mixture of 10 µL of TB Green Fast qPCR mix (CellAmp™ Direct TB Green® RT-qPCR Kit). The *OsActin* was selected as a housekeeping gene, and three biological replicates were analyzed. Primer sequences are listed in the Supplementary Table S1, together with all the other primers in this study.

## Subcellular localization of ROHAN

To investigate the subcellular localization of ROHAN, the *pROHAN:ROHAN:VENUS* and *pROHAN::ROHAN*$^{P211L}$*::VENUS* constructs were transformed into rice shoot protoplasts using polyethylene glycol (PEG)-mediated transformation[62]. Protoplasts isolated from rice and *pROHAN:ROHAN:VENUS* transgenic seedlings were observed using a confocal laser (Leica LSP8). YFP fluorescence was observed at 525 nm for emission and 514 nm for excitation.

## EDU staining

EDU staining was performed using an EdU kit (C10350, Click-iT EdU Alexa Fluor 488 HCS assay; Invitrogen), accordingly to the manufacturer's instructions. Roots of 4-days-old seedlings were immersed in 20 µM EDU solutions for 2 h and fixed for 30 min in 3.7% formaldehyde solution in phosphate buffer (pH 7.2) with 0.1% Tritonx-100, followed by 30 min of incubation with EDU detection cocktail. An Olympus MXV10 microscope with GFP channel was used to capture the images.

## Amino acid analysis

Wild-type and *rohan* plants were grown under different treatments for 4 days. Roots were collected for amino acid extraction as previously described[63]. Roots were collected in liquid nitrogen, then grinded and mixed manually. Samples were then transferred to 5 ml tubes, frozen with liquid nitrogen, and transferred to the lyophilizer (BILON, FD-2C, Shanghai, China) for 3 days. Lyophilized root tissues (~ 3 mg) were used for extraction with 80% methanol followed by incubation at 70℃ for 15 mins and shaking (600 *rpm*). Following centrifugation at 10,000 *g* for 15 min at room temperature, the supernatants were collected, the pellet was re-extracted with 20% methanol as described above. All supernatants were collected in a new pellet and dried in a Termovap Sample Concentrator MD200-1(Allsheng, China). The dried pellets were dissolved in 500 µL ultrapure water. 500 µL 4% 5-Sulfosalicylic acid dihydrate was added to re-dissolve followed by centrifugation at 12,000*g* for 15min at room temperature. The supernatants were collected and filtered by 0.22 µm water filter. The samples were analyzed with a LA8080 automatic amino acid analyzer (Hitachi, Tokyo, Japan). All steps were performed accordingly to the manufacturer's instructions.

## Photosynthesis parameter and seeds protein analysis

Simultaneous measurements of photosynthesis parameters were performed on light-adapted leaves with a LI-6,800 infrared gas analysis system. Prior to the measurements, the leaves were placed in a greenhouse at a photosynthetic photon flux density of 1,500 µmol·$m^{-2}s^{-1}$ with an ambient $CO_2$ concentration of 400 µmol/mol. After equilibration to a steady state, 0.8 s saturating pulses of light (~8,000 µmol·$m^{-2}s^{-1}$) were applied to measure the maximum ($F_m'$) and steady-state fluorescence ($F_s$); gas exchange parameters were recorded. The $\Phi_{PSII}$ was calculated as: $\Phi_{PSII} = (F_m' - F_s)/ F_m'$. Gas exchange parameters include net photosynthesis rate, stomatal conductance and transpiration rate. The seeds crude protein content was detected with a Near Infrared Spectroscope (NIRS) (DA7250, China).

## IAA content analysis

Germinated rice seedlings (3-day-old) were transferred to nutrient solution containing $NH_4^+$ or not. After 4 days of treatment, the roots were harvested and immediately frozen in liquid nitrogen. Auxin extraction procedure was conducted as described in[64]. Before chromatographic measurement, the dehydrated precipitate was re-suspended with 200 µL 80% MeOH. For chromatographic separations, UHPLC (Acquity UPLC-I-Class™, Waters, Milford, MA, USA) equipped with a reverse phase column (Waters BEH-C18 column, 2.1 × 50 mm, 1.7 µm) as the stationary phase was used, and FA in water (0.1%, v/v, buffer A) and methanol (buffer B) were employed as the mobile phase. Auxin extracts were subjected to a tandem quadrupole mass spectrometer, Waters Xevo TQ-S micro, for IAA quantification (Waters, Milford, MA, USA) equipped with an electrospray ionization (ESI) source. Data acquisition and processing were

performed using Masslynx software (version 4.1, Waters, Manchester, UK). The mass transitions were monitored as follows: *m/z* 176.07-130.00, external correction method based on IAA standards was used for relative IAA measurement.

Statistical analysis

The experiments performed in this study were repeated at least three times, and all the results were presented as the mean ± SD. SPSS software was used for statistical analysis. The significant difference between the two sets of data was determined by Student's *t*-test, whereas the difference among more than two sets of data was analyzed with one-way ANOVA followed by Duncan's multiple comparisons.

# References


1. Xu, G., Fan, X. & Miller, A. J. Plant Nitrogen Assimilation and Use Efficiency. *Annu. Rev. Plant Biol.* **63**, 153–182 (2012).

2. Subbarao, G. V. & Searchinger, T. D. Opinion: A "more ammonium solution" to mitigate nitrogen pollution and boost crop yields. *Proc. Natl. Acad. Sci.* **118**, 2107576118 (2021).

3. Li, B., Li, G., Kronzucker, H. J., Baluska, F. & Shi, W. Ammonium stress in *Arabidopsis*: signaling, genetic loci, and physiological targets. *Trends Plant Sci.* **19**, 107–114 (2014).

4. Chen, X. *et al.* Producingmore grain with lower environmental costs. *Nature* **514**, 486–489 (2014).

5. Qin, C. *et al.* GDP-mannose pyrophosphorylase is a genetic determinant of ammonium sensitivity in *Arabidopsis thaliana*. *Proc. Natl. Acad. Sci. U. S. A.* **105**, 18308–18313 (2008).

6. Li, B. *et al.* Arabidopsis plastid AMOS1/EGY1 integrates abscisic acid signaling to regulate global gene expression response to ammonium stress. *Plant Physiol.* **160**, 2040–2051 (2012).

7. Li, B. *et al.* Shoot-supplied ammonium targets the root auxin influx carrier AUX1 and inhibits lateral root emergence in *Arabidopsis*. *Plant, Cell Environ.* **34**, 933–946 (2011).

8. Li, G. *et al.* The *Arabidopsis* AMOT1/EIN3 gene plays an important role in the amelioration of ammonium toxicity. *J. Exp. Bot.* **70**, 1375–1388 (2019).

9. Coleto, I. *et al. Arabidopsis thaliana* transcription factors MYB28 and MYB29 shape ammonium stress responses by regulating Fe homeostasis. *New Phytol.* **229**, 1021–1035 (2021).

10. Hachiya, T. *et al.* Excessive ammonium assimilation by plastidic glutamine synthetase causes ammonium toxicity in *Arabidopsis thaliana*. *Nat. Commun.* **12**, 4944 (2021).

11. Jia, L. *et al.* Rice plants respond to ammonium stress by adopting a helical root growth pattern. *Plant J.* **104**, 1023–1037 (2020).

12. Jian, S. *et al.* NRT1.1-Related $NH_4^+$ Toxicity Is Associated with a Disturbed Balance between $NH_4^+$ Uptake and Assimilation. *Plant Physiol.* **178**, 1473–1488 (2018).

13. Sun, D. *et al.* Kinase SnRK1.1 regulates nitrate channel SLAH3 engaged in nitrate-dependent alleviation of ammonium toxicity. *Plant Physiol* **186**, 731–749 (2021).

14. Beeckman, F., Motte, H. & Beeckman, T. Nitrification in agricultural soils: impact, actors and mitigation. *Curr. Opin. Biotechnol.* **50**, 166–173 (2018).

15. Konishi, N. & Ma, J. F. Three polarly localized ammonium transporter 1 members are cooperatively responsible for ammonium uptake in rice under low ammonium condition. *New Phytol.* **232**, 1778–1792 (2021).

16. Hirano, T. *et al.* Inhibition of ammonium assimilation restores elongation of seminal rice roots repressed by high levels of exogenous ammonium. *Physiol. Plant.* **134**, 183–190 (2008).

17. Xuan, Y. H. *et al.* Indeterminate domain 10 regulates ammonium-mediated gene expression in rice roots. *New Phytol.* **197**, 791–804 (2013).

18. Li, G. *et al.* OsEIL1 protects rice growth under $NH_4^+$ nutrition by regulating OsVTC1-3-dependent N-glycosylation and root $NH_4^+$ efflux. *Plant. Cell Environ.* (2022) doi:10.1111/PCE.14283.

19. Jiao, X. *et al.* Promotion of BR Biosynthesis by miR444 Is Required for Ammonium-Triggered Inhibition of Root Growth. *Plant Physiol.* **182**, 1454–1466 (2020).

20. Kotogany, E., Dudits, D., Horvath, G. V & Ayaydin, F. A rapid and robust assay for detection of S-phase cell cycle progression in plant cells and tissues by using ethynyl deoxyuridine. *Plant Methods* **6**, 5 (2010).

21. Slocum, R. D. Genes, enzymes and regulation of arginine biosynthesis in plants. *Plant Physiol. Biochem.* **43**, 729–745 (2005).

22. Xia, J., Yamaji, N., Che, J., Shen, R. F. & Ma, J. F. Normal root elongation requires arginine produced by argininosuccinate lyase in rice. *Plant J.* **78**, 215–226 (2014).

23. Gaufichon, L., Reisdorf-Cren, M., Rothstein, S. J., Chardon, F. & Suzuki, A. Biological functions of asparagine synthetase in plants. *Plant Sci.* **179**, 141–153 (2010).

24. Hildebrandt, T. M., Nunes Nesi, A., Araújo, W. L. & Braun, H. P. Amino Acid Catabolism in Plants. *Mol. Plant* **8**, 1563–1579 (2015).

25. Zhang, S. *et al.* Nitrogen Mediates Flowering Time and Nitrogen Use Efficiency via Floral Regulators in Rice. *Curr Biol* **31**, 671-683 e5 (2021).

26. Luo, L. *et al.* Ammonium transporters cooperatively regulate rice crown root formation responding to ammonium nitrogen. *J. Exp. Bot.* (2022), erac059.

27. Kusano, M. *et al.* Metabolomics data reveal a crucial role of cytosolic glutamine synthetase 1;1 in coordinating metabolic balance in rice. *Plant J.* **66**, 456–466 (2011).

28. Hu, B. *et al.* Variation in NRT1.1B contributes to nitrate-use divergence between rice subspecies. *Nat. Genet.* **47**, 834–838 (2015).

29. Zhang, M. *et al.* Plasma membrane $H^+$-ATPase overexpression increases rice yield via simultaneous enhancement of nutrient uptake and photosynthesis. *Nat. Commun.* **12**, 735 (2021).

30. Kasper van Gelderen, Chiakai Kang & Ronald Pierik. Light Signaling, Root Development, and Plasticity. *Plant Physiol* **176**, 1049–1060 (2018).

31. Vega, A., O'Brien, J. A. & Gutierrez, R. A. Nitrate and hormonal signaling crosstalk for plant growth and development. *Curr. Opin. Plant Biol.* **52**, 155–163 (2019).

32. Hagen, G. & Guilfoyle, T. Auxin-responsive gene expression: genes, promoters and regulatory factors. *Plant Mol. Biol.* **49**, 373–385 (2002).

33. Yang, J. *et al.* Dynamic regulation of auxin response during rice development revealed by newly established hormone biosensor markers. *Front. Plant Sci.* **8**, 1–17 (2017).

34. Otvos, K. *et al.* Modulation of plant root growth by nitrogen source-defined regulation of polar auxin transport. *EMBO J.* **40**, e106862 (2021).

35. Kim, J. Y. *et al.* Identification of an ABCB/P-glycoprotein-specific inhibitor of auxin transport by chemical genomics. *J. Biol. Chem.* **285**, 23309–23317 (2010).

36. Teale, W. & Palme, K. Naphthylphthalamic acid and the mechanism of polar auxin transport. *J. Exp. Bot.* **69**, 303–312 (2018).

37. Kusano, M. *et al.* Cytosolic GLUTAMINE SYNTHETASE1;1 Modulates Metabolism and Chloroplast Development in Roots. *Plant Physiol.* **182**, 1894–1909 (2020).

38. Trovato, M., Funck, D., Forlani, G., Okumoto, S. & Amir, R. Editorial: Amino Acids in Plants: Regulation and Functions in Development and Stress Defense. *Front. Plant Sci.* **12**, 772810 (2021).

39. Li, G. *et al.* OsEIL1 protects rice growth under $NH_4^+$ nutrition by regulating OsVTC1-3-dependent N-glycosylation and root $NH_4^+$ efflux. *Plant. Cell Environ.* (2022) doi:10.1111/PCE.14283.

40. Jia, Z., Giehl, R. F. H. & von Wirén, N. Local auxin biosynthesis acts downstream of brassinosteroids to trigger root foraging for nitrogen. *Nat. Commun. 2021 121* **12**, 1–12 (2021).

41. Mazzoni-Putman, S. M., Brumos, J., Zhao, C., Alonso, J. M. & Stepanova, A. N. Auxin Interactions with Other Hormones in Plant Development. *Cold Spring Harb Perspect Biol* **13**, a039990 (2021).

42. Takagi, H. *et al.* MutMap accelerates breeding of a salt-tolerant rice cultivar. *Nat. Biotechnol.* **33**, 445–449 (2015).

43. Abe, A. *et al.* Genome sequencing reveals agronomically important loci in rice using MutMap. *Nat. Biotechnol.* **30**, 174–178 (2012).

44. Chen, S., Zhou, Y., Chen, Y. & Gu, J. fastp: an ultra-fast all-in-one FASTQ preprocessor. *Bioinformatics* **34**, i884–i890 (2018).

45. Li, H. & Durbin, R. Fast and accurate short read alignment with Burrows-Wheeler transform. *Bioinformatics* **25**, 1754–1760 (2009).

46. Tarasov, A., Vilella, A. J., Cuppen, E., Nijman, I. J. & Prins, P. Sambamba: fast processing of NGS alignment formats. *Bioinformatics* **31**, 2032–2034 (2015).

47. McKenna, A. *et al.* The Genome Analysis Toolkit: a MapReduce framework for analyzing next-generation DNA sequencing data. *Genome Res.* **20**, 1297–1303 (2010).

48. Pertea, M., Kim, D., Pertea, G. M., Leek, J. T. & Salzberg, S. L. Transcript-level expression analysis of RNA-seq experiments with HISAT, StringTie and Ballgown. *Nat. Protoc.* **11**, 1650–1667 (2016).

49. Dobin, A. *et al.* STAR: ultrafast universal RNA-seq aligner. *Bioinformatics* **29**, 15–21 (2013).

50. Kovaka, S. *et al.* Transcriptome assembly from long-read RNA-seq alignments with StringTie2. *Genome Biol.* **20**, 278 (2019).

51. Anders, S., Pyl, P. T. & Huber, W. HTSeq–a Python framework to work with high-throughput sequencing data. *Bioinformatics* **31**, 166–169 (2015).

52. Love, M. I., Huber, W. & Anders, S. Moderated estimation of fold change and dispersion for RNA-seq data with DESeq2. *Genome Biol.* **15**, 550 (2014).

53. Ma, X. *et al.* PlantGSAD: a comprehensive gene set annotation database for plant species. *Nucleic Acids Res.* **50**, D1456–D1467 (2021).

54. Wu, T. *et al.* clusterProfiler 4.0: A universal enrichment tool for interpreting omics data. *Innov. (N Y)* **2**, 100141 (2021).

55. Huang, X. *et al.* A map of rice genome variation reveals the origin of cultivated rice. *Nature* **490**, 497–501 (2012).

56. Wang, W. *et al.* Genomic variation in 3,010 diverse accessions of Asian cultivated rice. *Nature* **557**, 43–49 (2018).

57. Danecek, P. *et al.* The variant call format and VCFtools. *Bioinformatics* **27**, 2156–2158 (2011).

58. Cingolani, P. *et al.* A program for annotating and predicting the effects of single nucleotide polymorphisms, SnpEff: SNPs in the genome of Drosophila melanogaster strain w1118; iso-2; iso-3. *Fly* **6**, 80–92 (2012).

59. Hiei, Y., Komari, T. & Kubo, T. Transformation of rice mediated by *Agrabacterium tumefaciens*. *Plant Mol. Biol.* **35**, 205–218 (1997).

60. Xie, Y. *et al.* Cadmium stress suppresses lateral root formation by interfering with the root clock. *Plant Cell Environ.* **42**, 3182–3196 (2019).

61. De Smet, I. *et al.* An easy and versatile embedding method for transverse sections. *J. Microsc.* **213**, 76–80 (2004).

62. Tang, Z. *et al.* Knockdown of a rice stelar nitrate transporter alters long-distance translocation but not root influx. *Plant Physiol.* **160**, 2052–2063 (2012).

63. Guo, N. *et al. Oryza sativa* Lysine-Histidine-type Transporter 1 functions in root uptake and root-to-shoot allocation of amino acids in rice. *Plant J.* **103**, 395–411 (2020).

64. Novák, O., Pěnčík, A., Blahoušek, O. & Ljung, K. Quantitative Auxin Metabolite Profiling Using Stable Isotope Dilution UHPLC-MS/MS. *Curr. Protoc. plant Biol.* **1**, 419–430 (2016).

# Figures

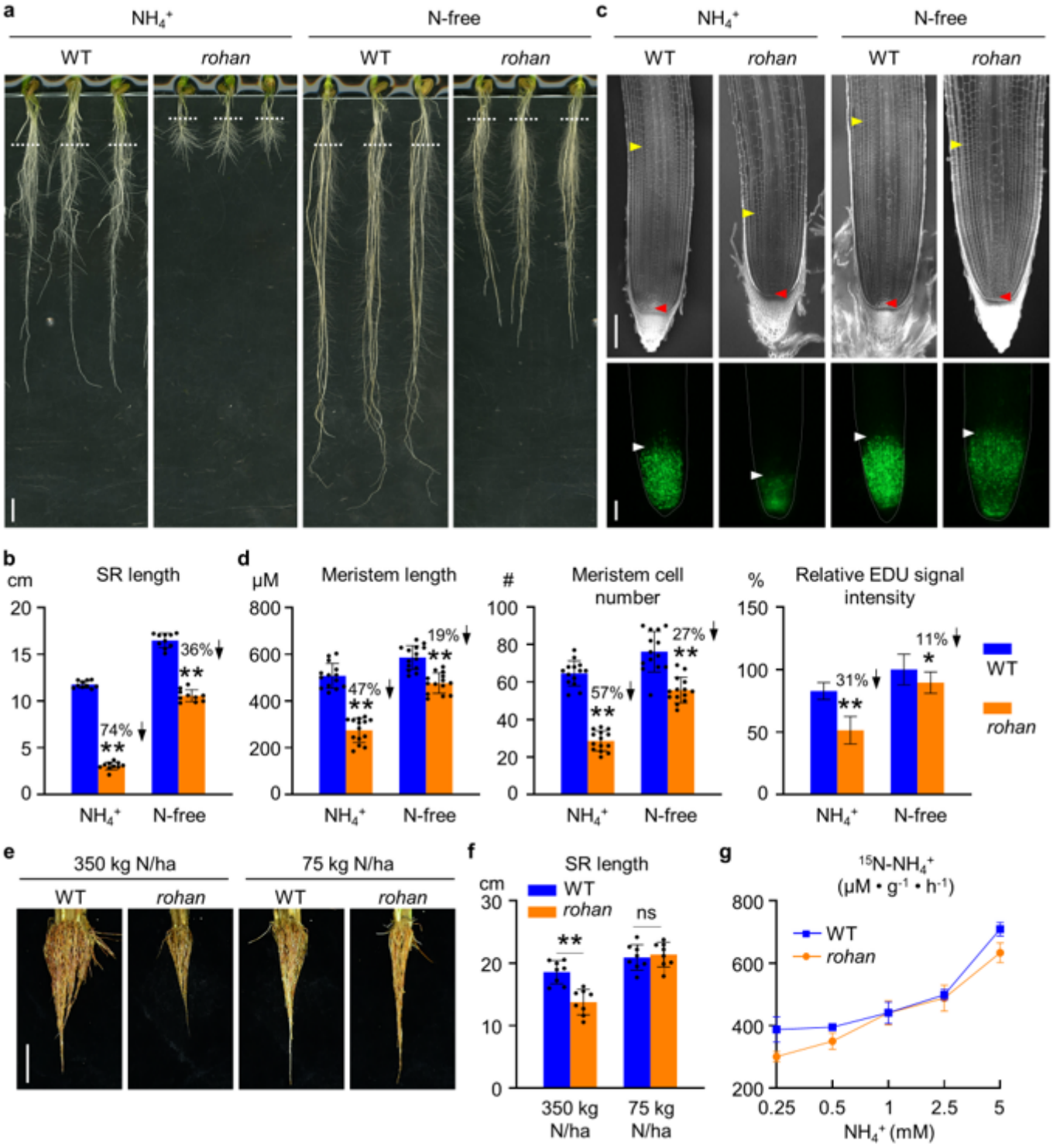


## Figure 1

### *rohan* mutant root growth is hypersensitive to $NH_4^+$.

**a** and **b,** Root phenotype **a** and seminal root (SR) length **b** of the wild-type (*Orzya sativa cv.* Wuyungeng7) and *rohan* mutant seedlings treated with or without 2.5 mM $NH_4^+$ for 15 days. The white dotted line indicates the position of the root tip when the seedlings were transferred to media supplied with or

without $NH_4^+$. Scale bars, 1 cm. Data represent the means ± s.d. (n ≥ 10 seedlings) (student's *t*-test, **P*<0.05, ***P* < 0.01 and ****P* < 0.001). **c**, Confocal images (upper panel) and Edu staining (lower panel) of the wild-type and *rohan* root meristem under N-free control and $NH_4^+$ treatments for 4 days. Red and yellow arrowheads indicate the stem cells and the start of transition zone, respectively. White arrowheads indicate the most shootward root tip Edu staining position. Scale bars, 100 μm. **d**, Quantification of root meristem length, cortical cell number and Edu signal intensity of the wild-type and *rohan* mutant seedlings shown in **c**. Data represent the means ± s.d. (n ≥ 10 seedlings). **e** and **f**, Root phenotype **e** and seminal root (SR) length **f** of the wild-type and *rohan* mutant plants grown in the paddy field with indicated N supplies. Scale bars, 5 cm. Data represent the means ± s.d. (n = 8 seedlings), and asterisks indicate significant differences between the two genotypes (student's *t*-test, **P*<0.05, ***P* < 0.01). **g**, $^{15}N$-$NH_4^+$ uptake in roots of the wild-type and *rohan* mutant seedlings after 10-min treatments with varying concentrations of $^{15}N$-$NH_4^+$. Data represent the means ± s.d. (n = 3 biological repeats).

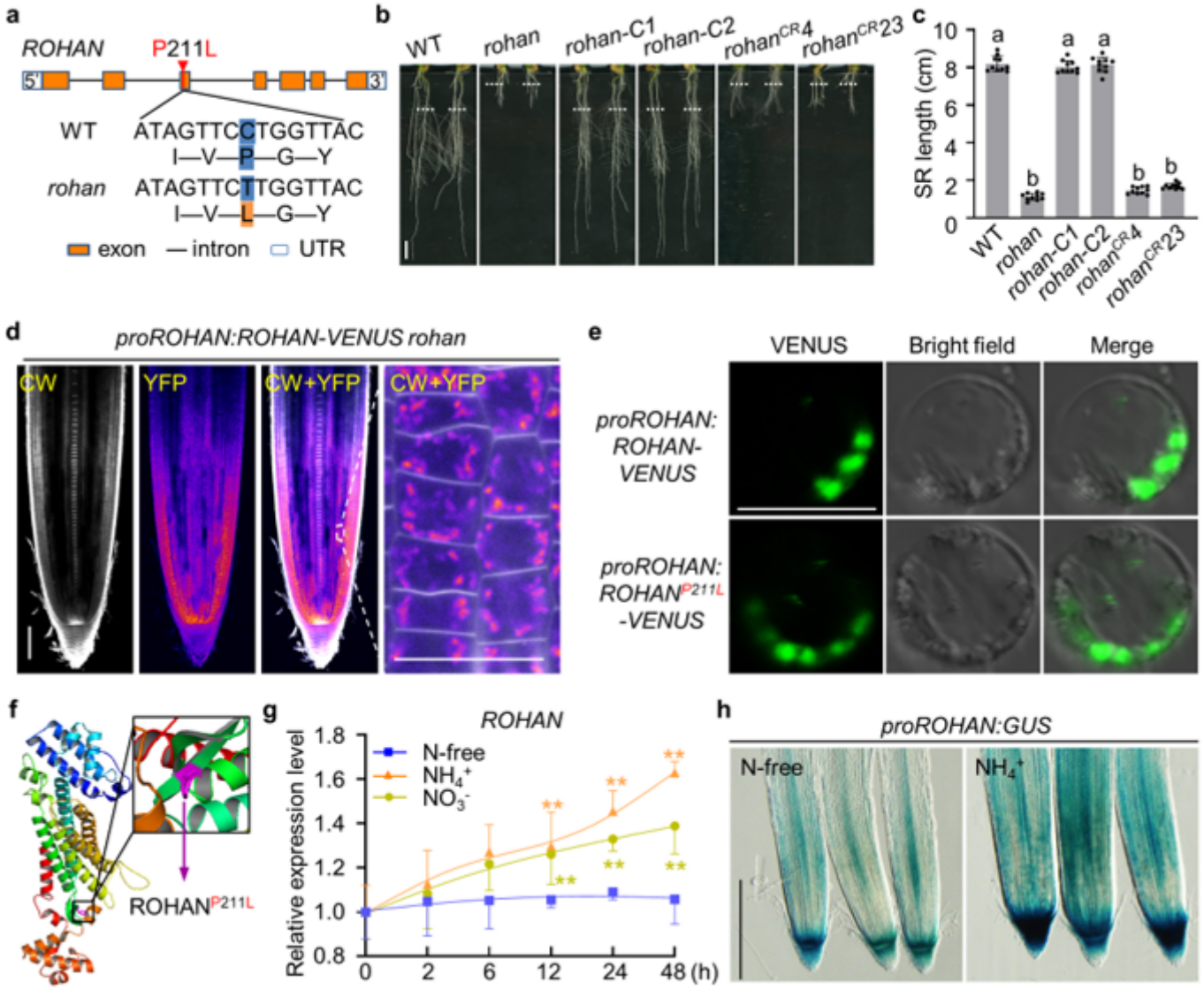


## Figure 2

***ROHAN* encodes a plastid-localized argininosuccinate lyase.**

**a**, Gene structure of *ROHAN*. Red arrowhead indicates the *rohan* mutation site. **b** and **c**, Root phenotype **b** and seminal roots (SR) length **c** of the indicated seedlings treated with 2.5mM $NH_4^+$ for 6 days. The mutant *rohan* was isolated from an EMS-mutagenized population of the wild-type *Orzya sativa cv.* Wuyungeng7. Furthermore, *rohan-C1* and *rohan-C2* are two independent complementary lines of *rohan*, and *rohan$^{CR}$4* and *rohan$^{CR}$23* are two independent CRISPR lines. The white dotted line indicates the position of the root tip when the seedlings were transferred to media supplied with $NH_4^+$. Scale bar, 1 cm. Data represent the means ± s.d. ($n \geq 10$ seedlings), and the letters denote significant differences between the genotype ($P < 0.05$ by one-way ANOVA followed by Tukey's test). **d**, *proROHAN:ROHAN-VENUS* expression in the root tip co-stained with calcofluor white (CW). Scale bars, 100 μm. **e**, Subcellular localization of ROHAN and mutated ROHAN (ROHAN$^{P211L}$) in rice protoplasts. Scale bar, 50 μm. **f**, Three-dimensional structure of ROHAN (PDB ID:ltj7) generated with the PyMOL software. The mutation site is shown in purple within the black pane. The purple arrow indicates the P211L amino acid replacement. **g**, Relative expression level of *ROHAN* at the root tip of wild-type seedlings under the treatments with N-free, $NH_4^+$ and $NO_3^-$ treatments over 48 hours. Data represent the means ± s.e. of three biological replicates, and asterisks indicate significant differences relative to N-free control condition (student's *t*-test, *$P$<0.05 and **$P < 0.01$). **h**, *proROHAN:GUS* expression at the root tip of wild-type plants treated with or without $NH_4^+$ for 24 hours. Scale bar, 1 mm.

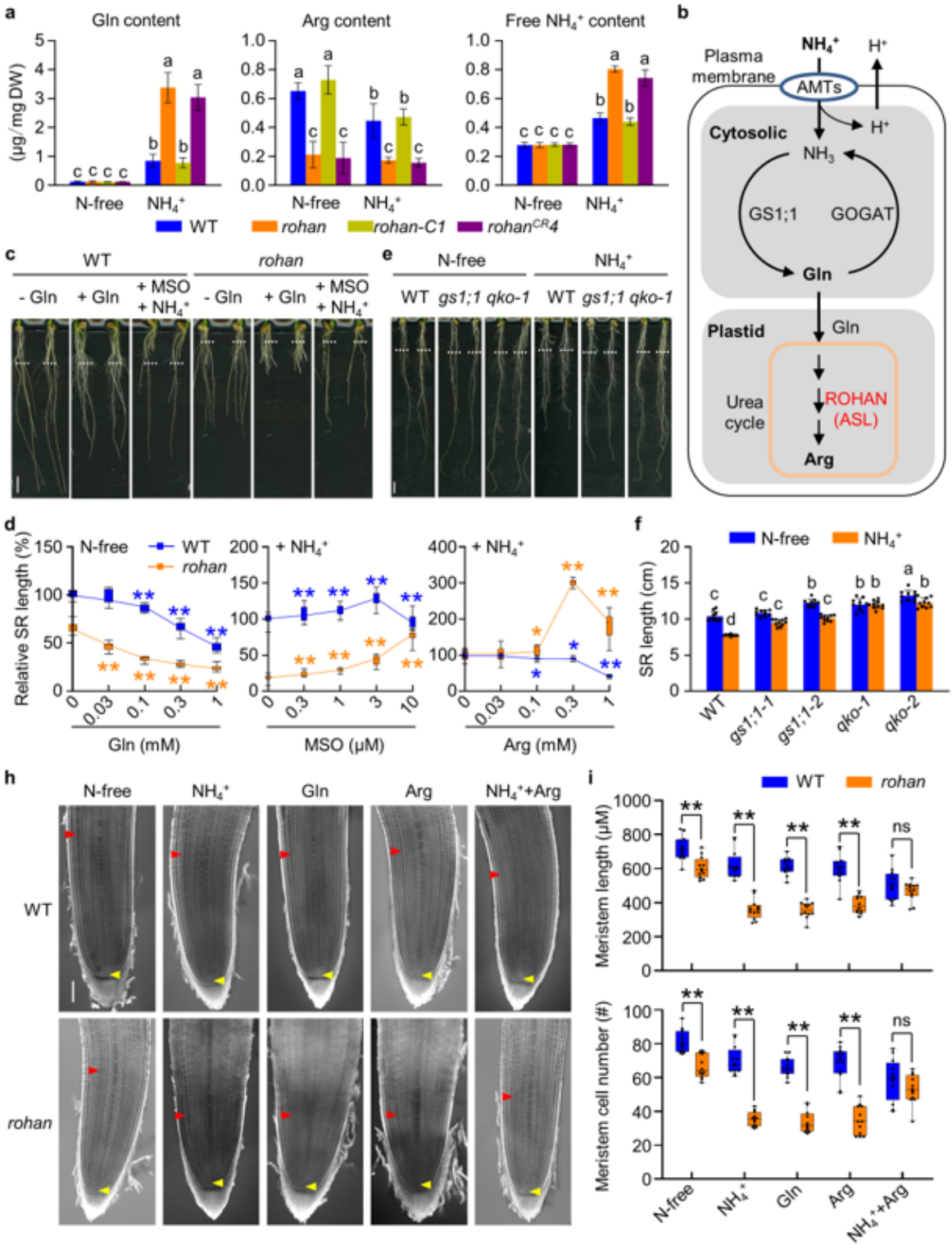


## Figure 3

### *rohan* is defective in the conversion of $NH_4^+$/Gln to Arg.

**a,** Content of Gln, Arg, and free $NH_4^+$ in the roots of the indicated seedlings treated with or without $NH_4^+$ for 6 days. The mutant *rohan* was isolated from an EMS-mutagenized population of the wild-type *Orzya sativa cv.* Wuyungeng7. Moreover, *rohan-C1* is a complementary line of the *rohan* while *rohan*$^{CR}$*4* is

CRISPR-generated mutant. Data represent the means ± s.d. of three biological replicates, and the letters denote significant differences ($P < 0.05$, by one-way ANOVA followed by Tukey's test). **b**, Proposed working model for the regulation of ROHAN in Gln and Arg metabolism. **c** and **d**, Root phenotype **c** and seminal roots (SR) length **d** of wild-type and *rohan* seedlings treated with Gln, MSO, and Arg, under indicated N conditions for 6 days. The following concentrations were used in **c**: 0.3 mM Gln and 10 μM MSO. The white dotted line indicates the position of the root tip when the seedlings were transferred to the new media supplied with the indicated chemicals. Scale bars, 1 cm. Data represent the means ± s.d. ($n \geq 10$ seedlings), and asterisks denote significant differences relative to chemical-free treatment (student's *t*-test, $*P<0.05$ and $**P < 0.01$). **e** and **f**, Root phenotype **e** and SR length **f** of Nipponbare, *gs1;1* glutamine synthetase 1 (GS1) mutant, and the *qko-1* quadruple mutant of ammonium transporters (AMTs) seedlings treated with or without 2.5 mM $NH_4^+$ for 6 days. The white dotted line indicates the position of the root tip when the seedlings were transferred to new media supplied with or without $NH_4^+$. Scale bars, 1 cm. Data represent the means ± s.d. ($n \geq 10$ seedlings), and the letters denote significant differences ($P < 0.05$, by one-way ANOVA followed by Tukey's test). **h,** Confocal images of wild-type and *rohan* root meristem under indicated treatments for 3 days. Red and yellow arrowheads indicate the stem cell and the start of transition zone, respectively. Scale bars, 100 μm. A concentration of 0.3 mM was used for both Gln and Arg treatments. **i**, Quantification of root meristem length and cortical cell number of in the wild-type and *rohan* seedlings shown in **h**. Data represent the means ± s.d. ($n \geq 10$ seedlings), and the asterisks indicate significant differences relative to the wild-type (student's *t*-test, $*P<0.05$ and $**P < 0.01$).

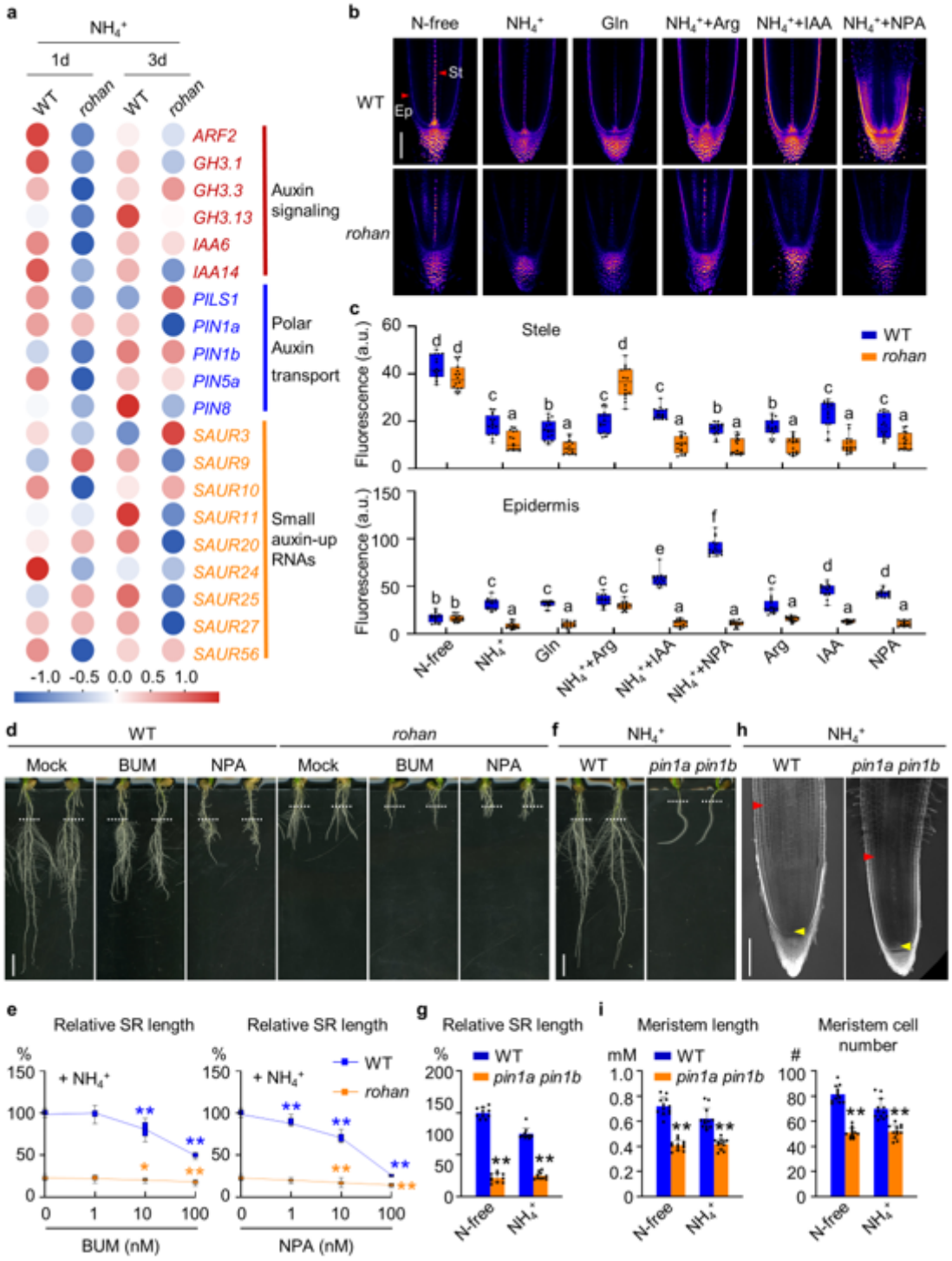


## Figure 4

### The root response of *rohan* mutant to $NH_4^+$ is mediated by auxin.

**a**, Heatmap of expression Z-scores of *ROHAN*-dependent differentially expressed genes that are relevant to auxin signal transduction and homeostasis. **b**, *DR5rev:3xVENUS-N7* expression in the root tips of wild-type (*Orzya sativa cv.* Wuyungeng7) and *rohan* seedlings grown under indicated treatments for 2 days. The red arrowheads indicate Ep (epidermis), St (stele). Scale bars, 100 μm. **c**, Quantification of

*DR5rev:3xVENUS-N7* signal in the root stele and epidermis of wild-type and *rohan* seedlings under indicated treatments. Data represent the means ± s.d. (n ≥ 10 seedlings), and letters denote significant differences ($P < 0.05$, by one-way ANOVA followed by Tukey's test). **d** and **e,** Root phenotype **d** and relative seminal roots (SR) length **e** of wild-type and *rohan* seedlings treated with NPA or BUM in the presence of 2.5 mM $NH_4^+$ for 6 days. The white dotted line indicates the position of the root tip when the seedlings were transferred to media supplemented with 100 nM BUM or 100 nM NPA. Scale bars, 1 cm. Data represent the means ± s.d. (n ≥ 10 seedlings), and the asterisks indicate significant differences relative to 0 nM BUM or NPA treatment (student's *t*-test, $*P<0.05$ and $**P < 0.01$). **f** and **g**, Root phenotype of wild-type and the auxin transporter double mutant *pin1apin1b* seedlings treated with 2.5 mM $NH_4^+$ **f** and relative SR length **g** of wild-type and *pin1apin1b* plants grown under N-free control condition or 2.5 mM $NH_4^+$ for 6 days. The white dotted line indicates the position of the root tip when the seedlings were transferred to new media containing the indicated treatments. Scale bars, 1 cm. Data represent the means ± s.d. (n ≥ 10 seedlings), and the asterisks indicate significant differences relative to the wild-type (student's *t*-test, $*P<0.05$ and $**P < 0.01$). **h**, Confocal images of wild-type and *pin1apin1b* mutant root meristem under 2.5 mM $NH_4^+$ treatments for 3 days. Red and yellow arrowheads indicate the stem cell and the start of transition zone, respectively. Scale bars, 100 μm. **i**, Quantification of root meristem length and cortical cell number and of the wild-type and *pin1apin1b* mutant seedlings shown in **h**. Data represent the means ± s.d. (n ≥ 10 seedlings), and the asterisks indicate significant differences relative to the wild-type (student's *t*-test, $*P<0.05$ and $**P < 0.01$).

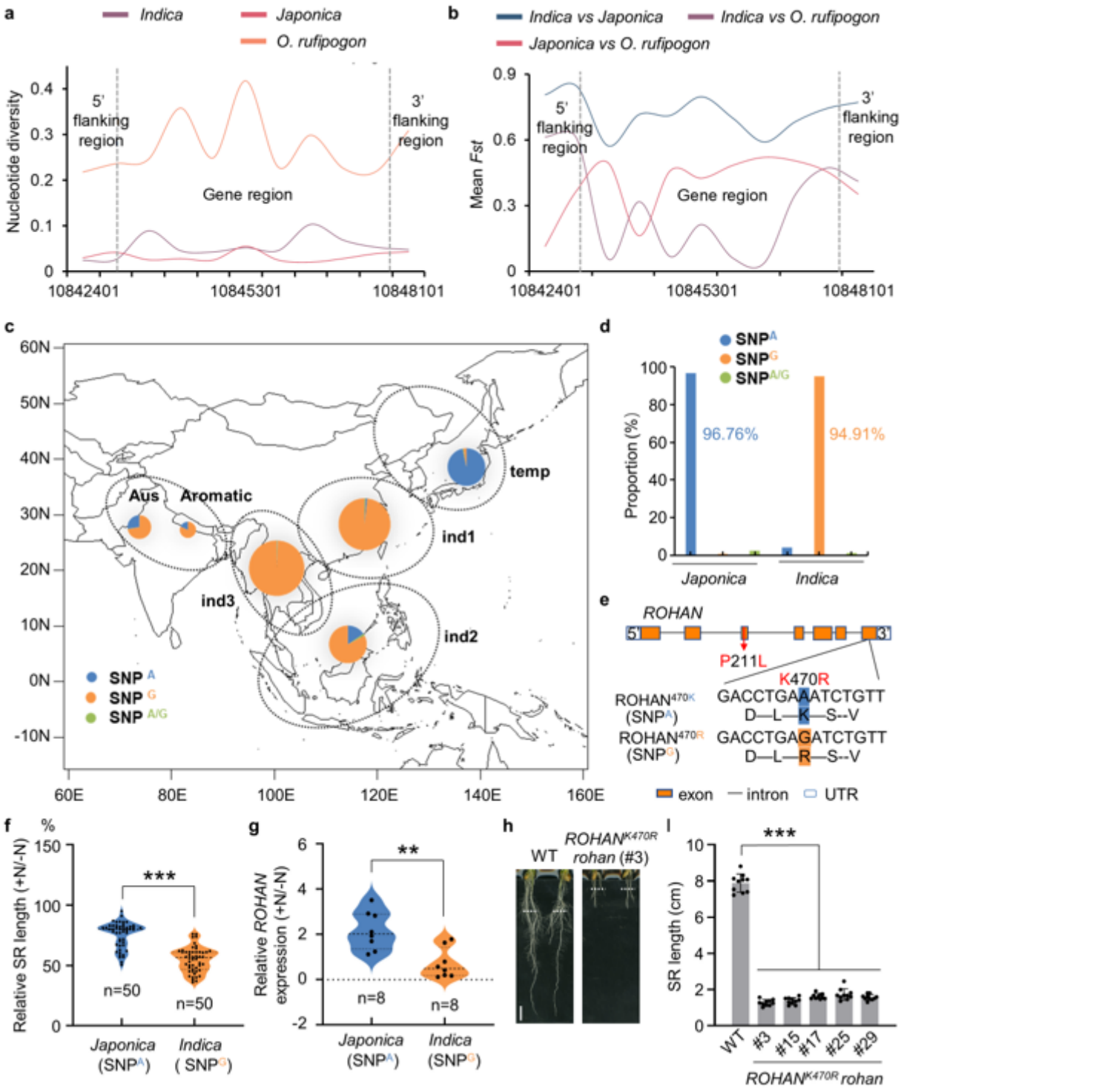


## Figure 5

**Genetic variation of *ROHAN* is associated with its regulatory role in root response to $NH_4^+$.**

**a**, Nucleotide diversity(π) of *ROHAN* gene and flanking regions between different rice subspecies. **b**, Mean *Fst* value of *ROHAN* gene and flanking regions between different rice subspecies. **c**, Geographic distribution of of the SNP(Chr3:10847318)'s allele frequency in different rice varieties based on the 3,000 Rice Genome database. **d**, Distribution of the SNP(Chr3:10847318) in *Japonica* and *Indica* rice

subspecies based on the 3,000 Rice Genome Project database. **e**, Amino acid change caused by the SNP mutant (A<-G). **f**, Comparison of relative seminal roots (SR) length (+N/-N) between *Japonica* and *Indica* ssb. seedlings grown under 2.5 mM $NH_4^+$ (+N) or N-free (-N) condition for 6 days. Data represent the means ± s.d. (n = 50 cultivars for either *Japonica* or *Indica* subspecies, ≥ 10 seedlings per cultivar), and the asterisk indicates significant difference (student's *t*-test, ***$P$ < 0.001). **g**, Comparison of relative gene expression (+N/-N) of *ROHAN* in roots between *Japonica* (n = 8 cultivars) and *Indica* subspecies (n = 8 cultivars) grown under 2.5 mM $NH_4^+$ (+N) or N-free (-N) conditions. Data represent the means ± s.e. of three biological replicates, and the asterisk indicates significant difference between two subspecies (student's *t*-test, **$P$ < 0.01). **h** and **i**, Root phenotype **h** and the seminal root (SR) length **i** of the wild-type (*Orzya sativa cv.* Wuyungeng7) and of five independent complementary lines of *rohan* mutant carrying K470R substitution, treated with 2.5 mM $NH_4^+$ for 6 days. The white dotted line indicates the position of the root tip when the seedlings were transferred to media supplied with 2.5 mM. Scale bars, 1 cm. Data represent the means ± s.d. (n ≥ 10 seedlings), and the asterisk indicates significant difference between two subspecies (student's *t*-test, ***$P$ < 0.001).

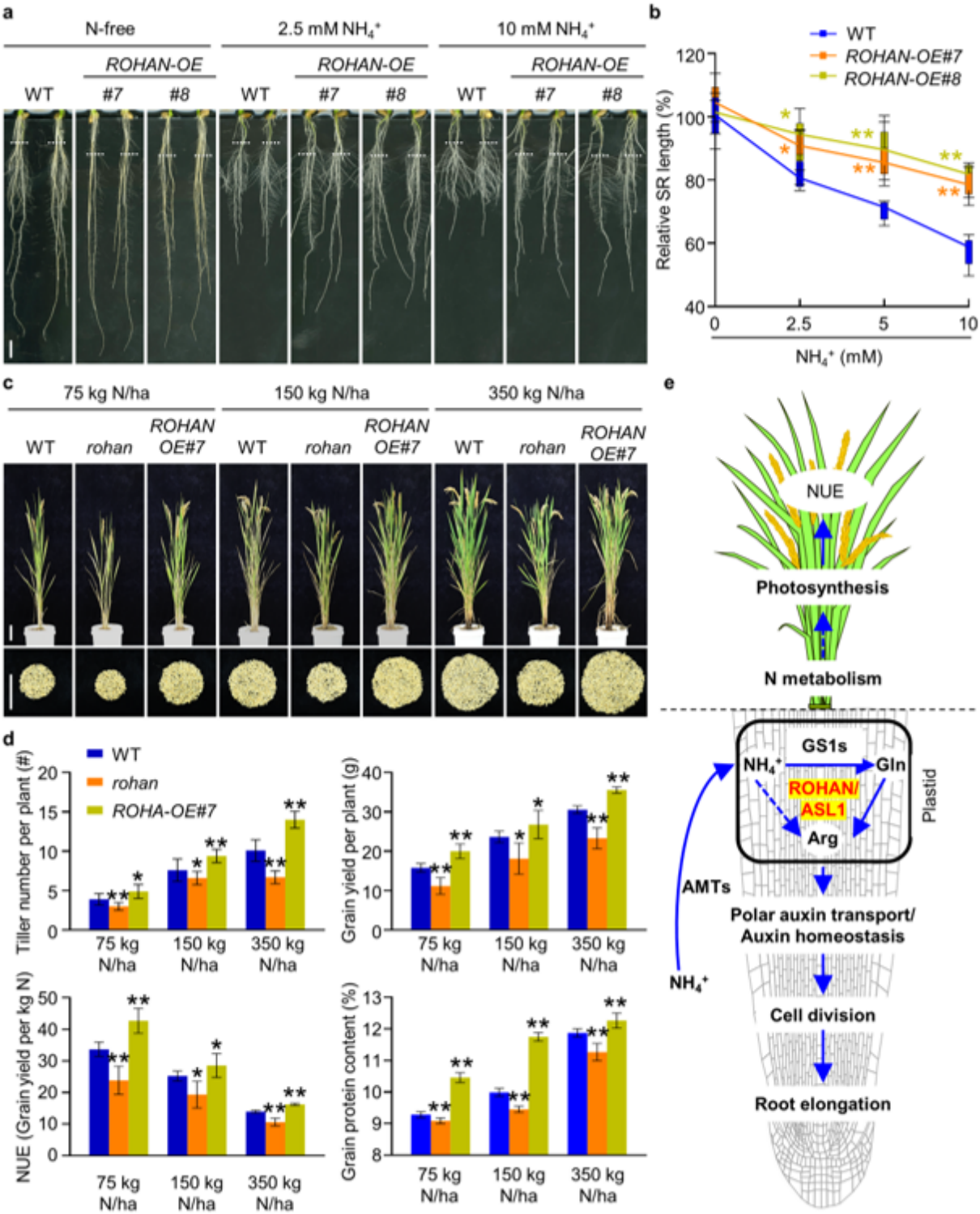


## Figure 6

**_ROHAN_ expression determines the rice tolerance to $NH_4^+$ toxicity and nitrogen use efficiency.**

**a** and **b**, Root phenotype **a** and relative seminal roots (SR) length **b** of the wild-type (*Orzya sativa cv.* Wuyungeng7 and of two independent transgenic *ROHAN* overexpression lines treated with varying concentrations of $NH_4^+$ for 6 days. The white dotted line indicates the position of the root tip when the

seedlings were transferred to media supplemented with $NH_4^+$. Scale bar, 1 cm. Data represent the means ± s.d. (n ≥ 10 seedlings), and the asterisks indicate significant differences relative to WT under each concentration of $NH_4^+$ (student's *t*-test, **P*<0.05 and ***P* < 0.01). **c**, Gross morphology (upper panel) and total grains per plant (lower panel) of the wild-type, the *rohan* mutant and *ROHAN* overexpression lines grown in the field with at the indicated N supplies. Scale bars, 10 cm. **d**, Quantification of indicated agronomic traits and grain crude protein content in the wild-type, the *rohan* mutant and the *ROHAN* overexpression line shown in **c**. Data represent the means ± s.d. (n ≥ 10 seedlings), and the asterisks indicate significant differences relative to the wild-type under each concentration of $NH_4^+$ (student's *t*-test, **P*<0.05 and ***P* < 0.01). **e**, Proposed working model for the role of *ROHAN* in coordinating nitrogen metabolism and hormone signal to regulate root elongation under high ammonium. NUE: Nitrogen Use Efficiency; GS1: Glutamine Synthetase 1; ASL1: Argininosuccinate lyase; AMTs: Ammonium transporters.

## Supplementary Files

This is a list of supplementary files associated with this preprint. Click to download.

- SupplementaryInformationtosubmit.docx